Available online at www.sciencedirect.com

ScienceDirect

Ceramics International 40 (2014) 4085–4093

CERAMICS INTERNATIONAL

www.elsevier.com/locate/ceramint

Ferroelectric and structural instability of (Pb,Ca)TiO_3 thin films prepared in an oxygen atmosphere and deposited on LSCO thin films which act as a buffer layer

D.S.L. Pontes[a], F.M. Pontes[b,*], Marcelo A. Pereira-da-Silva[c], M. Zampieri[a], A.J. Chiquito[d], P.S. Pizani[e], E. Longo[a,f]

[a]*LIEC – Department of Chemistry, Universidade Federal de São Carlos, Via Washington Luiz, Km 235, P.O. Box 676, 13565-905 São Carlos, São Paulo, Brazil*
[b]*Department of Chemistry, Universidade Estadual Paulista – Unesp, P.O. Box 473, 17033-360 Bauru, São Paulo, Brazil*
[c]*Institute of Physics of São Carlos, USP, São Carlos 13560-250, São Paulo, Brazil*
[d]*NanoLab – Department of Physics, Universidade Federal de São Carlos, Via Washington Luiz, Km 235, P.O. Box 676, 13565-905 São Carlos, São Paulo, Brazil*
[e]*Department of Physics, UFSCar, Via Washington Luiz, Km 235, CEP-13565-905 São Carlos, São Paulo, Brazil*
[f]*Institute of Chemistry, Universidade Estadual Paulista – Unesp, Araraquara, São Paulo, Brazil*

Received 4 July 2013; received in revised form 15 August 2013; accepted 15 August 2013
Available online 27 August 2013

Abstract

Structural, microstructural and ferroelectric properties of $Pb_{0.90}Ca_{0.10}TiO_3$ (PCT10) thin films deposited using $La_{0.50}Sr_{0.50}CoO_3$ (LSCO) thin films which serve only as a buffer layer were compared with properties of the thin films grown using a platinum-coated silicon substrate. LSCO and PCT10 thin films were grown using the chemical solution deposition method and heat-treated in an oxygen atmosphere at 700 °C and 650 °C in a tube oven, respectively. X-ray diffraction (XRD) and Raman spectroscopy results showed that PCT10 thin films deposited directly on a platinum-coated silicon substrate exhibit a strong tetragonal character while thin films with the LSCO buffer layer displayed a smaller tetragonal character. Surface morphology observations by atomic force microscopy (AFM) revealed that PCT10 thin films with a LSCO buffer layer had a smoother surface and smaller grain size compared with thin films grown on a platinum-coated silicon substrate. Additionally, the capacitance versus voltage curves and hysteresis loop measurement indicated that the degree of polarization decreased for PCT10 thin films on a LSCO buffer layer compared with PCT10 thin films deposited directly on a platinum-coated silicon substrate. This phenomenon can be described as the smaller shift off-center of Ti atoms along the *c*-direction ⟨001⟩ inside the TiO_6 octahedron unit due to the reduction of lattice parameters. Remnant polarization (P_r) values are about 30 μC/cm^2 and 12 μC/cm^2 for PCT10/Pt and PCT10/LSCO thin films, respectively. Results showed that the LSCO buffer layer strongly influenced the structural, microstructural and ferroelectric properties of PCT10 thin films.

Keywords: Thin films; Buffer layers; $Pb_{1-x}Ca_xTiO_3$; Chemical synthesis

1. Introduction

Ferroelectric thin film perovskites such as $PbTiO_3$ (PTO), Pb(Zr_xTi_{1-x})O_3 (PZT), $Ba_{1-x}Sr_xTiO_3$ (BST), $BaTiO_3$ (BTO), $Pb_{1-x}Sr_xTiO_3$ (PST) and $Pb_{1-x}Ca_xTiO_3$ (PCT) have attracted significant interest due to their simple crystal structure, potential application in ultrahigh density memory devices, tunable microwave devices, infrared sensors, etc [1–6]. Among them, the solid solution of $Pb_{1-x}Ca_xTiO_3$ (PCT) is a well known ferroelectric material [7,8] and is regarded as a promising material for piezoelectric sensors and uncooled pyroelectric infrared detectors. Recently, much research has been devoted to the preparation of PCT thin films on oxide single crystal substrates such as $SrTiO_3$, $LaAlO_3$, SiO_2 and MgO by various deposition techniques to investigate their structural, microstructural, optical and ferroelectric properties [9,10]. However, few investigations have been reported on the successful preparation of PCT thin films directly on an oxide buffer layer by a chemical wetting method.

The crystallographic orientation as well as microstructural and electrical properties of ferroelectric thin films are influenced by the deposition method, bottom electrodes, substrates surface,

*Corresponding author. Tel.: +55 14 3103 6135; fax: +55 14 3103 6088.
E-mail address: fenelon@fc.unesp.br (F.M. Pontes).

0272-8842/$ - see front matter © 2013 Elsevier Ltd and Techna Group S.r.l. All rights reserved.
http://dx.doi.org/10.1016/j.ceramint.2013.08.063

atmosphere, thickness and buffer layers [11]. Recently, several groups published studies on the relationship between electrical behavior and phase and crystallographic orientation by the introduction of appropriate oxide electrodes or buffer layers such as $SrRuO_3$, $LaNiO_3$, CeO_2, TiO_2, ZnO, ITO, $SrTiO_3$, $La_{1-x}Sr_xMnO_3$, $La_{0.07}Sr_{0.93}SnO_3$, $La_{1-x}Sr_xCoO_3$, etc. [12–14]. Several researchers reported that the formation of a deleterious pyrochlore phase could be effectively suppressed by the insertion of an adequate buffer layer between platinum-coated silicon substrates and PZT, PMN–PT and PT thin films [15,16]. Since some ferroelectric thin films deposited directly on platinum coated silicon substrates often contain a considerable amount of a deleterious pyrochlore phase which is characterized by poor electrical properties; i.e., a lower dielectric constant and remnant polarization. Takahara et al. [16] reported that PZT thin films deposited directly on a platinum-coated MgO single crystal substrate by a pulsed laser deposition (PLD) technique resulted in the predominant pyrochlore phase. However, Takahara et al. demonstrated that the pyrochlore phase completely disappeared when $SrTiO_3$ (STO) thin films acting as buffer layer were inserted into the PZT/Pt interface [16]. Actually, efforts have been made by Jiang et al. [15] to grow phase-free pyrochlore PMN–PT thin films. In this study, a PMN–PT thin film was grown on buffer layers of LSCO/CeO_2/YSZ deposited on a silicon substrate using PLD.

Therefore, it has been suggested that the selection of an appropriate buffer layer is crucial in deciding the phase formation, microstructure, structure and electrical properties in ferroelectric thin film technology. Currently, there are several deposition techniques for fabricating oxide electrodes or buffer layers such as laser ablation, sputtering, and sol–gel [17–19]. Tang et al. have shown that PCT thin films on $LaNiO_3$ coated fused quartz and Si substrates maintain good dielectric and ferroelectric properties [20]. Effects of $LaNiO_3$ and CeO_2 buffer layers deposited directly on a platinum electrode surface on the crystallographic orientation, microstructure and electrical properties of BZT thin films have been studied extensively by Gao et al. [21]. Among these oxide buffer layers, pseudocubic perovskite $La_{1-x}Sr_xCoO_3$ thin films have been intensively studied and have shown a strong influence as a buffer layer [22–24]. Cheng et al. [25] reported the effects of $La_{0.5}Sr_{0.5}CoO_3$ (LSCO) and $La_{0.5}Sr_{0.5}MnO_3$ (LSMO) buffer layers on the polarization switching of $Pb_{1-x}Sr_xTiO_3$/LSMO/Pt–Si and $Pb_{1-x}Sr_xTiO_3$/LSCO/Pt–Si thin films. To our knowledge, there are few reports regarding PCT thin films on platinum-coated silicon substrates with LSCO buffer layers and their structural, microstructural and ferroelectric properties have not been investigated.

In this work, we investigated the influence of LSCO thin films as buffer layers on the structural, microstructural and ferroelectric properties of $Pb_{0.90}Ca_{0.10}TiO_3$ (PCT10) thin films prepared by a chemical solution deposition (CSD) method. In addition, these properties were compared with properties of PCT10 thin films deposited directly on a platinum-coated silicon substrate. The combined results of XRD, Raman spectroscopy, AFM and ferroelectric measurements indicate that the insertion of LSCO thin films introduced an interesting and fruitful way to investigate the role of a buffer layer in PCT10 samples. In addition, the dependence of the observed ferroelectric behavior in PCT10 samples is described within a framework where the LSCO buffer layer plays a fundamental role. In fact, properties of PCT10 samples can be artificially tailored to easily control type buffer layer.

2. Experimental procedure

$Pb_{0.90}Ca_{0.10}TiO_3$ (PCT10) thin films used in this study were produced by a chemical solution deposition method. Details of the preparation method can be found in the literature [26].

$La_{0.50}Sr_{0.50}CoO_3$ (LSCO) thin films as buffer layers were prepared using a CSD method. Starting chemical reagents were cobalt carbonate ($CoCO_3$), strontium carbonate ($SrCO_3$) and lanthanum acetate ($La_2(CH_3COO)_2 \cdot 2H_2O$) from Alfa Aeasar Co. Water, citric acid and ethylene glycol were used as solvent, chelating and polymerizing agents, respectively, to prepare the solution. First, cobalt citrate was formed by the dissolution of cobalt carbonate in a water solution of citric acid (70–80 °C) under constant stirring to homogenize the cobalt citrate aqueous solution. Second, strontium carbonate was added in a stoichiometric quantity to the cobalt citrate aqueous solution. After the homogenization of this solution, lanthanum acetate was also slowly added. The complex was stirred well for several hours at 80 °C to produce a clear, homogenous solution. Then the solution containing Co, Sr and La was homogenized, and ethylene glycol was added to promote citrate polymerization by a polyesterification reaction. With continued heating at 90 °C, the solution became more viscous, although without any visible phase separation. The molar ratio between cobalt cations, strontium and lanthanum was 2:1:1; the citric acid/ethylene glycol was fixed at 60:40 (mass ratio). With continued heating at 80–90 °C, the solution became more viscous, albeit devoid or any visible phase separation. Finally, the viscosity of the deposition solution was adjusted to 10 mPa/s by controlling the water content.

LSCO buffer layers were prepared by a spin coating technique on Pt/Ti/SiO_2/Si substrates at 6000 rpm for 30 s. Each spin-coated LSCO buffer layer was subsequently baked at 150 °C on a hot plate for 20 min to remove any residual solvents. A two-stage heat treatment was carried out as follows: an initial heating at 400 °C for 4 h at a heating rate of 5 °C/min in an oxygen atmosphere to pyrolyze the organic materials followed by heating at 700 °C for 2 h at a heating rate of 5 °C/min for crystallization in an oxygen atmosphere in a tube oven. Each layer was pyrolyzed at 400 °C and crystallized at 700 °C before the next layer was deposited. These coating/drying operations were repeated until the desired thickness was obtained.

Additionally, PCT10 thin films were deposited on LSCO buffered Pt/Ti/SiO_2/Si and Pt/Ti/SiO_2/Si substrates, respectively. First, PCT10 thin films were deposited on the LSCO-buffered Pt/Ti/SiO_2/Si substrate using a commercial spinner operating at 6000 rpm for 30 s (spin-coater KW-4B, Chemat Technology). After each coating, the thin films were heat-treated at 400 °C for 4 h and then at 650 °C for 2 h at a heating rate of 5 °C/min in an

oxygen atmosphere. Each layer was pyrolyzed at 400 °C and crystallized at 650 °C before the next layer was deposited. The film thickness was controlled by adjusting the number of coatings; the coating/drying operation was repeated until the desired thickness was achieved.

Second, PCT10 thin films were deposited on a $Pt/Ti/SiO_2/Si$ substrate using the same coating process and heat treatment described for PCT10 thin films on LSCO.

PCT10 and LSCO thin films were then structurally characterized by XRD in the 2θ–θ scan mode which was recorded on a Rigaku D/Max 2400 diffractometer. Thicknesses of thin films were characterized using field emission-scanning electron microscopy (FE-SEM) (FEG-VP Zeiss Supra 35) on a freshly fractured film/substrate cross-section. AFM was used to obtain a bi- and tri-dimensional image reconstruction of the sample surface. These images provided an accurate analysis of the sample surface and the quantification of parameters such as roughness and grain size. A Digital Instruments Multi-Mode Nanoscope IIIa was used for these experiments.

Raman measurements were taken at room temperature with a T-64000 Jobin-Yvon triple-monochromator coupled to a charge-coupled detector (CCD). An optical microscope with a 100× objective was used to focus the 514.5 nm line of a Coherent Innova 70 argon laser onto the sample. The laser output power was maintained at about 15 mW.

Ferroelectric properties were measured in metal–ferroelectric–metal (MFM) and metal–ferroelectric–buffer layer–metal (MFBLM) architecture (see Fig. 1). The capacitance or dielectric constant versus voltage (C–V) curves were characterized using a Hewlett-Packard (4192 LF) impedance analyzer with the capacitance value measured using a small a.c. signal of 10 mV at 100 kHz. The hysteresis loop measurements were carried out on the films with a Radiant Technology RT6000HVS at a measured frequency of 60 Hz. The loops were traced using the "CHARGE 5" program; this program is in the software of the RT6000HVS operated in a virtual ground mode test. To measure electrical properties, Au dot electrodes (4.8×10^{-4} cm^2 area) were deposited using a shadow mask by an evaporation process on the fired thin film surfaces as top electrodes. All measurements were conducted at room temperature.

3. Results and discussions

Fig. 2a shows XRD patterns of PCT10 thin films on a platinum-coated silicon substrate with and without LSCO thin films as the buffer layer which were prepared by the CSD method. In the same graph, we also show the XRD pattern of a polycrystalline LSCO thin film for comparison. Fig. 2b shows XRD patterns for PCT10 and LSCO bulk powders for comparison. Fig. 2a(1) confirms that LSCO thin films display a polycrystalline pseudo-cubic perovskite phase only without any other crystalline phase [27]. XRD patterns indicate that PCT10 thin films deposited on a platinum-coated silicon substrate and on a LSCO buffer layer possess a polycrystalline nature without preferential orientation and exhibit a single perovskite phase without any impurity phase (see Fig. 2a(2) and (3)) which is consistent with the report by Song et al. [23,28] for $BaTiO_3$ and $Ba(Sn_{0.05}Ti_{0.95})O_3$ thin films deposited on LSCO buffered $Pt/Ti/SiO_2/Si$ substrates. Similar behavior was revealed by Cheng et al. for $Pb_{0.60}Sr_{0.40}TiO_3$ thin films deposited on Pt-coated silicon substrates using either $La_{0.50}Sr_{0.50}CoO_3$ or $La_{0.50}Sr_{0.50}MnO_3$ thin films as buffer layers which were prepared by PLD [25].

Additionally, PCT10 samples deposited directly on a platinum-coated silicon substrate demonstrate that (001)/(100) and (101)/(110) doublets are well separated (see Fig. 2a(3)) with strong tetragonal distortion. Surprisingly, PCT10 samples grown on a LSCO buffer layer show a distinct behavior (see Fig. 2a(2)). Structural changes of the thin films as a function of the LSCO buffer layer are clearly evident, and the tetragonality of the thin films is pronouncedly decreased; i.e., an overlap of the diffraction peaks and, as consequence, a lower crystal c/a ratio due to a lattice matching between PCT10 thin films and the LSCO buffer layer. XRD patterns indicate that lattice parameters of these samples (PCT10 on platinum, PCT10 on a LSCO buffer layer and a LSCO buffer layer) are $a_{PCT10/Pt}$=3.899 Å, $c_{PCT10/Pt}$=4.094 Å, $a_{PCT10/LSCO}$=3.913 Å, $c_{PCT10/LSCO}$=4.045 Å and $a_{LSCO}=c_{LSCO}$=3.836 Å. This result confirms that the mismatch (MM) between the PCT10 sample and the LSCO buffer layer is MM_a=1.96% and MM_c=5.16% while MM between the PCT10 sample and the platinum-coated silicon substrate is only MM_a=−0.72% and MM_c=3.67%. However,

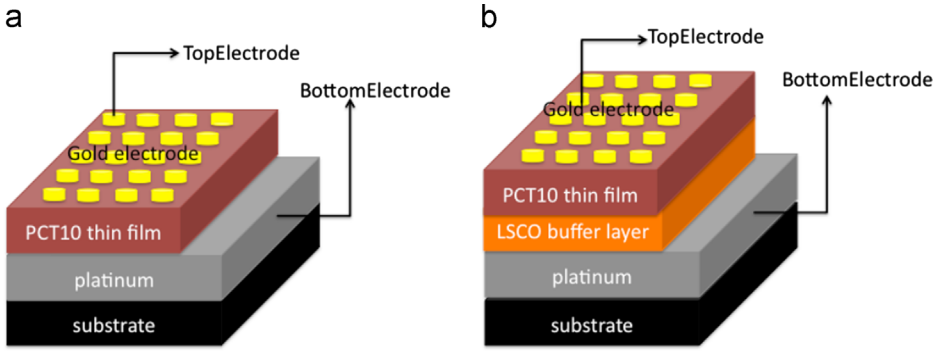

Fig. 1. Schematic diagrams show (a) MFM architecture and (b) MFBLM architecture. In MFBLM architecture, LSCO thin films act as a buffer layer and platinum bottom electrodes.

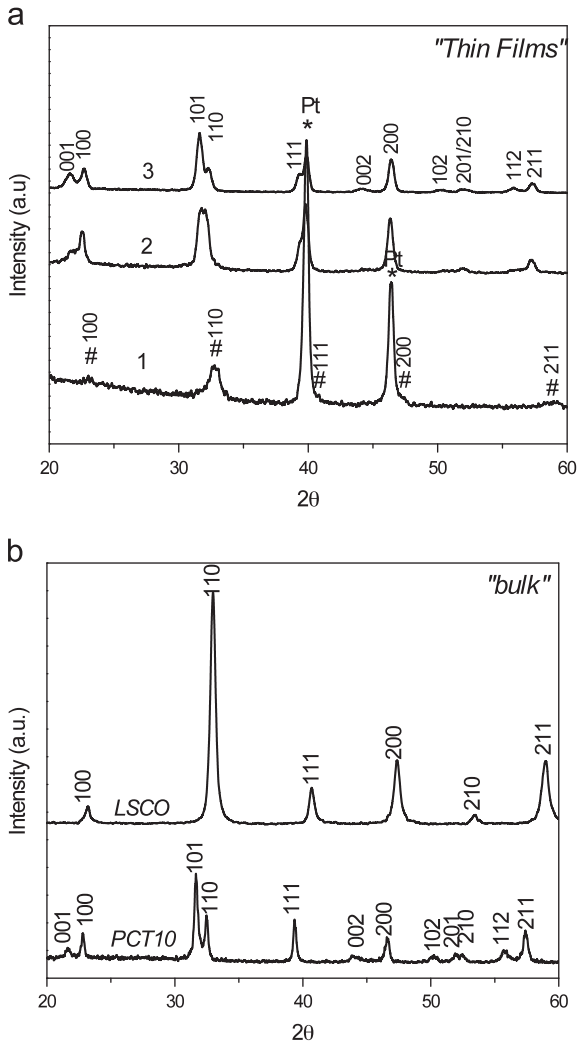

Fig. 2. XRD patterns: (a) platinum-coated silicon substrate: 1) LSCO thin films on platinum-coated silicon substrate; 2) PCT10 thin films on LSCO buffer layers; and 3) PCT10 thin films on a platinum-coated silicon substrate; and (b) LSCO and PCT10 bulk materials.

the lattice *MM* between the PCT10 and the LSCO is much larger than the *MM* between PCT10 and platinum. This result implies that the stress induced by LSCO buffer layers effectively influences the PCT10 sample crystal structure (see Fig. 2a). On the other hand, when the buffer layer was changed to platinum, the lattice *MM* values were reduced. These facts suggest that samples are almost fully relaxed; i.e., this surface decreases the interfacial energy between PCT10 and platinum by reducing the lattice *MM*. Additionally, the PCT10 sample crystal structure on platinum has nearly the same lattice parameter as the polycrystalline PCT10 bulk powder (a_{Bulk}=3.883 Å and c_{Bulk}=4.108 Å). Fig. 3 shows a schematic diagram of the different stress situations that the PCT10 thin film undergoes under different lattice surface *MMs*.

Raman spectroscopy was used to corroborate the structural study realized by XRD. Raman spectroscopy is a powerful tool to study short- and medium-range structural changes and, in particular, to detect slight deviations from the tetragonal-to-cubic (or vice-versa) structures that often occur in the class of perovskite-type compounds. Furthermore, the Raman mode shift is proportional to the magnitude of residual stress in thin films [29,30]. According to many authors, polar transverse-optical (TO) lattice vibrational modes (*ferroelectric soft mode* or simply *soft-mode*) are heavily polar in the ferroelectric crystal structure and are considered as a driving force for ferroelectric instability and/or phase transition [31,32]. Moreover, $PbTiO_3$ and $PbTiO_3$-based solid solutions are archetypes of tetragonal perovskite ferroelectrics with 12 well known optical vibrational modes. In PCT, the lowest E(1TO) and A1 (1TO) phonon modes (*soft-mode*) in the tetragonal perovskite system correspond to vibrations of the lead atoms with respect to slightly distorted TiO_6 octahedra units along the *x* or *y* direction and along the *z* direction, respectively, where the displacement polarization is determined by tetragonal distortion (*c*/*a*). Since the *soft-mode* distortion or instability is an order parameter of the ferroelectric and structural instability, it is usually very sensitive (i.e, to the stress, grain size, and lattice) in thin films.

As discussed above, the *soft-mode* behavior investigation in ferroelectric crystal structures is very useful to better correlate their structural characteristics with ferroelectric properties.

In this study, we investigate the effects of LSCO thin films acting as buffer layers between PCT10 thin films and the platinum bottom electrode that can induce significant modifications in the Raman signature of PCT10 thin films (see Fig. 4). The LSCO layer is Raman inactive and prevents the incident laser excitation from impinging on the substrate [33]. In the same graph, for comparison, we also show Raman spectra for the PCT10 bulk powder. Furthermore, drastic changes in Raman spectra can be observed for PCT10/LSCO architecture; first, only diffused, weak and broader peaks are visible in PCT10 thin films in the LSCO buffer layer (see Fig. 4c). Moreover, the disappearance and/or displacement of various Raman modes for lower wavenumbers indicates that PCT10 thin films on LSCO buffer layers underwent a drastic short- and medium-range structural change at room temperature. The optical phonon frequency shift in thin films to lower values is thought to be similar to the effect of hydrostatic pressure observed by many authors in bulk powders [34]. Second, A_1(1TO) and *E*(1*TO*) phonon modes (*soft-mode*) are markedly altered with respect to the PCT10 bulk powder and appear more frequently at lower wavenumbers in PCT10/LSCO samples than in PCT10/Pt and bulk samples which clearly indicates that there is a decrease in the tetragonal character for PCT10 samples on LSCO buffer layers. The larger upward shift in the *soft-mode* in PCT10/LSCO samples with respect to PCT10/Pt samples is due to the larger *MM* between PCT10 and LSCO layers as compared to the *MM* between PCT10 and platinum with a small grain size, stress and decreased lattice parameters. Effects of LSCO buffer layers on the *soft-mode* frequency of PLT thin films have also been reported by Zhu et al. [35]. All these observations confirm that PCT10/LSCO samples are under residual stress. Similar to E(TO) modes, A_1(3TO), A_1(2TO) and A_1(1TO) modes are also shifted to lower wavenumbers in comparison with A_1 PCT10/Pt modes.

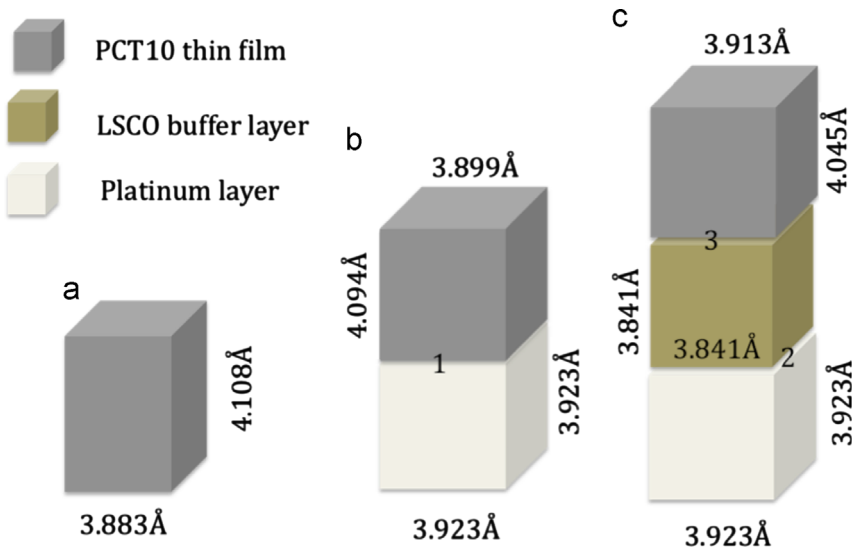

Fig. 3. Schematic diagrams showing: (a) a strain-free PCT10 bulk powder; (b) PCT10 thin films on platinum (1 – unstressed or almost fully relaxed; condition $a_{film} \cong a_{substrate}$); and (c) LSCO thin films on platinum (2 – under tensile strain; condition $a_{substrate} > a_{film}$) and PCT10 thin films on LSCO buffer layer (3 – under compressive strain; condition $a_{film} > a_{substrate}$); 1, 2, and 3 are interface conditions.

Therefore, the broadening and larger shift to lower band wavenumbers and the dramatic decrease in their intensities produced a structural ferroelectric instability and implies a weakening of short-range ferroelectric order which is in agreement with the decrease in tetragonality obtained from XRD response.

Contrarily, PCT10 thin films deposited under identical conditions on a platinum-coated silicon substrate exhibited intense Raman mode characteristics for the perovskite phase only (see Fig. 4b); all Raman features are clearly resolved. The intensity of E(TO) and A(TO) modes is much higher for these samples which probably originates from the large grain size, larger tetragonality and mainly from the fact that samples are almost fully relaxed (unstressed) with respect to PCT10 bulk powder (see lattice parameters and Raman spectra in Fig. 4a). However, we cannot rule out smaller residual stress between PCT10 thin films and the platinum bottom electrode. For example, linewidths and broader optical phonon frequencies are sensitive to microstrutural changes, stress, thickness, temperature and pressure; this result corroborates the XRD analysis. In addition, the Raman spectrum at room temperature is in agreement with the literature and shows all Raman active modes [36]. By fitting measured spectra and decomposing the fitted curves into individual Lorentzian components, the peak position of each component (i.e., the natural frequency of each Raman active mode) was obtained for PCT10/LSCO, PCT10/platinum samples and PCT10 bulk powder for comparison. These data for optical phonon frequencies and their mode symmetry assignments are summarized in Table 1.

All the proposed procedures discussed above can simultaneously or individually produce degradation of PCT10 thin films ferroelectric properties on LSCO buffer layers. Nevertheless, it appears plausible to speculate that, considering a relationship between tetragonal structure changes and the ferroelectric order (polarization or polar soft-mode), we can

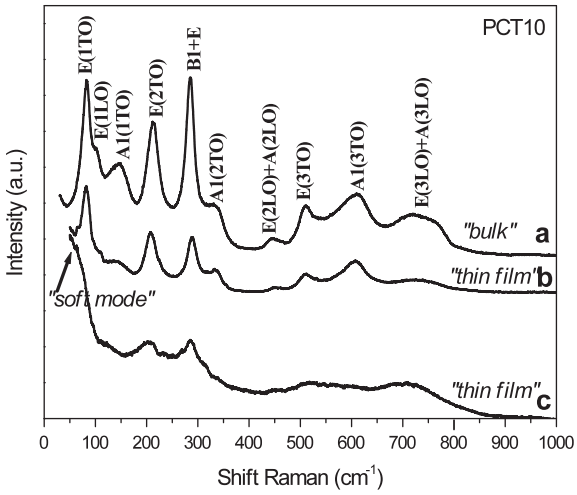

Fig. 4. Room temperature Raman spectra of: (a) a PCT10 bulk powder; (b) PCT10 thin films on platinum-coated silicon substrates; and (c) PCT10 thin films on LSCO buffer layers.

Table 1
Observed phonon frequencies (cm^{-1}) for PCT10 powder bulk (*a*), PCT10 thin films on platinum bottom electrode (*b*) and PCT10 thin films on LSCO buffer layer (*c*).

Mode symmetry	PCT10 (*a*)	PCT10 (*b*)	PCT10 (*c*)
E(1TO)	84	80	59
E(1LO)	104	105	–
A_1(1TO)	145	142	–
E(2TO)	212	208	202
B1+E	284	289	286
A_1(2TO)	334	334	298
E(2LO)+A(2LO)	448	454	451
E(3TO)	508	510	523
A_1(3TO)	610	607	–
E(3LO)+A(3LO)	719/766	727	706

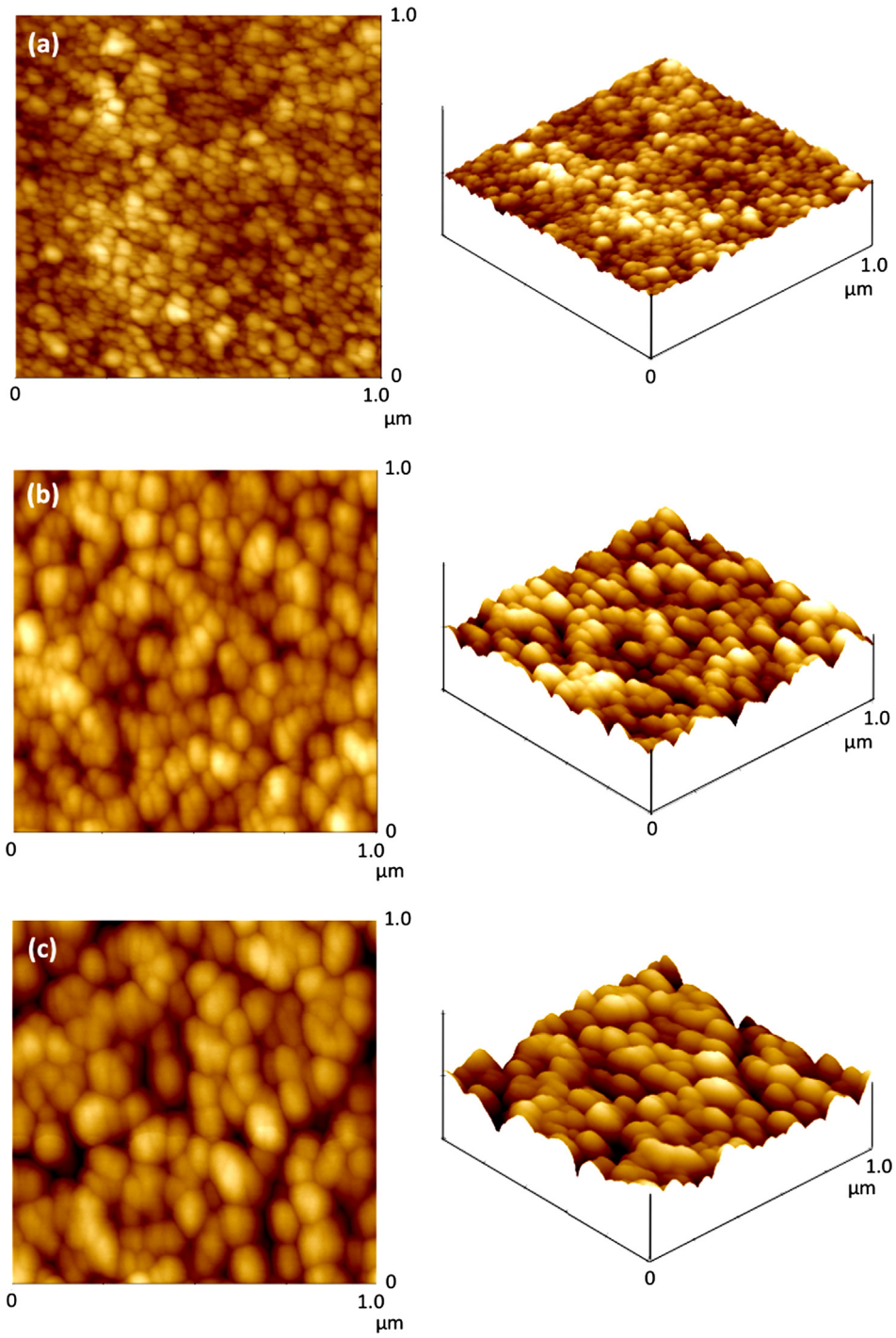

Fig. 5. AFM images of PCT10 and LSCO thin film surface morphology: (a) LSCO thin films as buffer layers on platinum-coated silicon substrates; (b) PCT10 thin films on LSCO buffer layers; and (c) PCT10 thin films on platinum-coated silicon substrates.

expect smaller remnant polarization for PCT10/LSCO samples than for PCT10/Pt samples (to be discussed in the next paragraphs).

Fig. 5 shows surface morphologies obtained by AFM in the contact mode of PCT10 thin films on LSCO and platinum-coated silicon substrates and LSCO buffer layers. The LSCO thin film surface on a platinum-coated silicon substrate is very smooth with an average surface roughness of 2 nm and a grain size of approximately 15–20 nm. The buffer layer effects on the PCT10 thin film microstructure is equally significant and generally supports inferences drawn from XRD and Raman spectroscopy studies. Both thin films display good microstructural uniformity concerning the absence of discontinuities (pinholes or microcracks) and low surface roughness. However, PCT10 thin films on LSCO buffer layers have a smoother surface and smaller grain size than films deposited directly on

platinum-coated silicon substrates. These observations can be attributed to the different interactive strength between the buffer layers and the PCT10 thin films which directly influences the nucleation and the grain growth mechanism. At the same time, the PCT10 film average grain size on LSCO buffer layers and platinum-coated silicon substrates were approximately 50–60 nm and 90–100 nm, respectively. Root-mean-square roughness values for PCT10 thin films on platinum-coated silicon substrates and LSCO buffer layer were 6 and 4 nm, respectively. Qin et al. [20] reported BST thin films grown on Pt/Ti/SiO_2/Si substrates with and without LSCO buffers layers using PLD. These authors reported that BST thin films with LSCO buffer layers had a smoother surface and a smaller grain size than thin film buffer layers on Pt substrates. Chae et al. [37] researched PZT thin films grown on Pt/Ti/SiO_2/Si substrates with and without $LaNiO_3$ (LNO) buffers layers by the sol–gel technique and revealed that the PZT thin film average grain size on LNO buffers layers is smaller than that of the grain size on metal electrode (platinum substrate) films; this result is consistent with our results.

Cross-sectional measurements reveal that the LSCO buffer layer on a platinum-coated silicon substrate is about 100 nm in thickness whereas PCT10 thin films on a platinum-coated silicon substrate and on LSCO buffer layer are about 210 and 270 nm thick, respectively (not shown here).

In principle, these drastic structural changes in PCT10 thin films should have a significant impact on ferroelectric properties of these samples. To establish the structure–ferroelectric property correlation in these samples, their capacitance–voltage (*C–V* curves) polarization-electric field (hysteresis loop) responses were investigated at room temperature. The $PbTiO_3$ prototype has a non-centrosymmetric tetragonal crystal structure with a strong spontaneous polarization along the *c*-axis. Therefore, the application of extrinsic or intrinsic stress can drastically change *c* lattice parameters values (polarization *c*-axis) which results in different degrees of polarization.

Fig. 6 displays *C–V* or dielectric constant versus applied voltage curves obtained from PCT10 samples on different surfaces (a platinum-coated silicon substrate and a LSCO buffer layer). The butterfly shape exhibited by both samples established their ferroelectric nature but with a different magnitude. Similar results were reported by Simões et al. [38]; a narrowing of the *C–V* curve was obtained for (Bi,La)FeO_3 thin films deposited on LSCO/Pt substrates.

PCT10 thin films on platinum-coated silicon substrates revealed a larger splitting between up-sweep/down-sweep measurements which characterizes a strong spontaneous polarization; i.e., strong short- and long-range ferroelectric order and suggests that the shift of Ti atoms inside the TiO_6 octahedral results in intense noncentrosymmetric ferroelectric order and is expected to show a high remnant polarization value. In the other words, Ti atoms have a larger shift within the octahedron (TiO_6 unit) in the *c* direction (polarization axis) for the PCT10/Pt sample as compared with the PCT10/LSCO sample. This result is based on lattice parameter values in the *c* direction: $c_{PCT10/Pt}=4.094$ Å $> c_{PCT10/LSCO}=4.045$ Å as well as on Raman measurements.

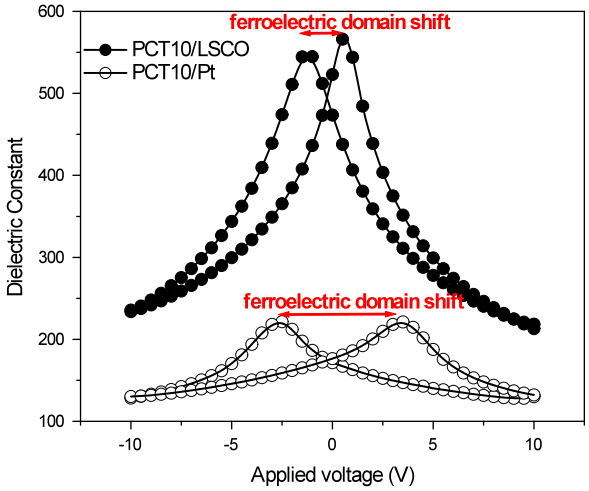

Fig. 6. Dielectric constant versus applied voltage curves for PCT10 thin films with and without LSCO buffer layers (measured at 100 kHz). The red arrow shows a different magnitude for the ferroelectric domain shift (For interpretation of the reference to color in this figure legend, the reader is referred to the web version of this article).

On the contrary, for the LSCO buffer layer, the butterfly shape of curves was smaller than curves for PCT10 thin films deposited directly on platinum. As indicated by XRD and Raman spectroscopy, PCT10 samples on LSCO buffer layers result in a lower lattice parameter and a small octahedral distortion. Importantly, the reduction of lattice parameters also resulted in a decrease in ionic displacement; i.e., Ti atoms with a smaller shift within the octahedron (TiO_6 unit) in the *c* direction (polarization axis). As a result, the smallest ferroelectric domain shifts occur; i.e., a weakening of the short-range ferroelectric order.

On the other hand, in a recent investigation, only the absence of splitting was observed in *C–V* curves for $Pb_{1-x}Ca_xTiO_3$ thin films on a platinum-coated silicon substrate in a composition near $x=0.40$ [26].

Fig. 7 shows the hysteresis loop response of PCT10 thin films. The hysteresis loop character is an indication of ferroelectricity in both samples which is consistent with *C–V* curves. These curves indicate that PCT10 thin films on a platinum-coated silicon substrate with and without LSCO thin films as buffer layers which are prepared by the CSD method have a ferroelectric nature, but the properties are quite different for the same PCT10 sample on a different growth surface. In addition, both samples show a slight shift toward positive voltages as a consequence of a high built-in field common in thin films. Remnant polarization (P_r) and coercive field (E_c) values are estimated to be approximately 30 μC/cm^2, 250 kV/cm and 12 μC/cm^2, 126 kV/cm for the PCT10 thin films on a platinum-coated silicon substrate without and with LSCO thin films as buffer layer, respectively. Notice that the remnant polarization of thin films with a LSCO buffer layer are smaller than the corresponding values of thin films which were prepared directly on platinum. This phenomenon can be ascribed to the following factors: (i) small grain size; (ii) small shift off-center of Ti atoms along the *c*-direction ⟨001⟩

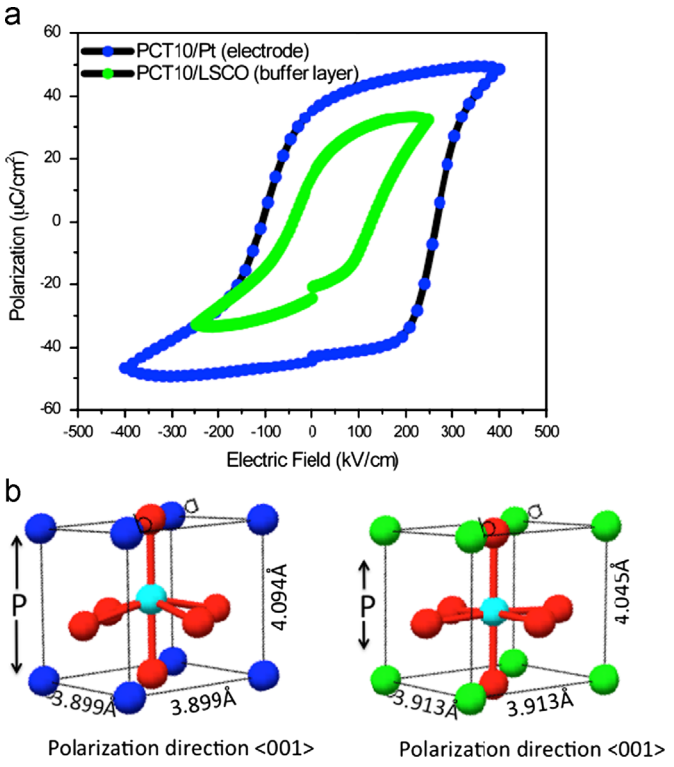

Fig. 7. (a) *P–E* hysteresis loops measured with 8 V driving voltage for PCT10 thin films on platinum electrode (blue curve) and on LSCO buffer layers (green curve); (b) schematic polarization of states diagram showing the large shift off-center of Ti atoms along the *c*-direction $<001>$ for PCT10 on platinum and a small shift off-center of Ti atoms along the *c*-direction $<001>$ for PCT10 on LSCO buffer layers. Pb or Ca (blue or green), O (red) and Ti (cyan) (Illustration is not in scale) (For interpretation of the references to color in this figure legend, the reader is referred to the web version of this article).

inside a TiO_6 octahedron unit; (iii) reduction of the tetragonality due to residual stress in thin films caused by a higher *MM* between thin film interfaces/LSCO buffer layers; and (iv) weakening short-range polar distortion (short-range ferroelectric order). All these factors facilitate a lower remnant polarization. This result is consistent with Raman data where the *soft-mode* is taken to be a result of a short- and long-range polarization balance (ferroelectric order); i.e., *soft-mode* instability causes degradation in ferroelectric properties.

Notably, PCT10 thin films deposited directly on a platinum-coated silicon substrate have a larger saturated hysteresis loop with a higher remnant polarization value. This result is due to factors such as: (i) larger grain size; (ii) high degree of tetragonality observed mainly by Raman spectroscopy; (iii) as a consequence, the situation is more conducive to a large shift off-center of Ti atoms along the *c*-direction ⟨001⟩ inside the TiO_6 octahedron unit; and (iv) increase in the mobility for ferroelectric domains (180° domains) caused by increased lattice parameters (*c*-axis). As mentioned above, XRD and Raman data for PCT10/Pt samples exhibit enhanced tetragonal distortion which induces a strong polarization out-of-plane (*c* direction).

Additionally, Fig. 7b shows the magnitude of polarization as a function of the shift of off-center Ti atoms along the *c*-direction for PCT10 thin films with and without LSCO buffer layers.

4. Conclusion

In summary, results clearly revealed the significant impact of LSCO thin films acting as buffer layers on structural, microstructural and ferroelectric properties for PCT10 thin films. A comparison of XRD data with results of the Raman spectra analysis shows a weak distortion of the tetragonal unit cell in PCT10 thin films deposited directly on LSCO buffer layers as a result of the larger *MM* between PCT10 and LSCO layers. The XRD analysis indicated a smaller tetragonal character for PCT10 thin films on LSCO buffer layers than on platinum-coated silicon substrates. In addition, for both thin films, no evidence of secondary phases was found. AFM images reveal that PCT10 thin film growth on LSCO buffer layers exhibited homogeneous grain distribution, atomically smooth surfaces and small grain sizes with no pinholes. Raman spectroscopy reveals that most phonon frequencies remarkably shift to a lower frequency for PCT10 thin films on LSCO buffer layers as compared with PCT10 thin films deposited directly on platinum. This frequency downshift behavior can be attributed to compressive stress in thin films. In our case of PCT10 thin films on platinum, phonon frequencies are found at a higher frequency due to larger tetragonality.

Combined results of *C–V* curves and hysteresis loop measurements demonstrate that remnant polarization decreased for PCT10 thin films on LSCO buffer layers. We believe that the observed polarization reduction in our PCT10/LSCO sample is due to a small grain size, a small shift off-center of Ti atoms inside the TiO_6 octahedron unit, a reduction in lattice parameters in the *c*-direction and polar *soft-mode* instability.

However, structural, microstructural and ferroelectric property measurements show that LSCO thin films as buffer layers have considerable influence on the corresponding tetragonality, grain size, surface roughness and ferroelectric properties of PCT10 thin films.

Acknowledgments

This work was financially supported by the Brazilian agencies FAPESP, CNPq and CAPES. We thank CEPID/CMDMC/INCTMN. FAPESP process nos. 08/57150-6 and 11/20536-7.

References

[1] X. Yang, X. Wu, W. Ren, P. Shi, X. Yan, H. Lei, Xi Yao, Effects of $LaNiO_3$ buffer layers on preferential orientation growth and properties of $PbTiO_3$ thin films, Ceramics International 34 (2008) 1035–1038.

[2] B. Wen, Y. Zhang, X. Liu, L. Ma, X. Wang, Fatigue improvement in modified lead zirconate titanate ceramics through employment of $La_{0.8}Sr_{0.2}MnO_3$ buffer layers, Ceramics International 39 (2013) 219–225.

[3] F. Stemme, M. Bruns, H. Geßwein, M. Schroeder, M. Sazegar, M. D. Drahus, R.-A. Eichel, F. Paul, C. Azucena, J.R. Binder, Fabrication and characterization of iron and fluorine co-doped BST thin films for microwave applications, Journal of Materials Science 48 (2013) 3586–3596.

[4] J. Hiltunen, D. Seneviratne, H.L. Tuller, J. Lappalainen, V. Lantto, Crystallographic and dielectric properties of highly oriented $BaTiO_3$

films: influence of oxygen pressure utilized during pulsed laser deposition, Journal of Electroceramics 22 (2009) 395–404.
[5] Q.G. Chi, H.F. Zhu, J.Q. Lin, C.T. Chen, X. Wang, Y. Chen, Q.Q. Lei, Crystallization behaviors and electric properties of $(Pb_{0.8}Ca_{0.2})TiO_3$ thin films prepared by a sol–gel route, Applied Surface Science 273 (2013) 702–705.
[6] X. Lei, D. Remiens, N. Sama, Y. Chen, C. Mao, X. Dong, G. Wang, Dielectric, ferroelectric and piezoelectric properties of 100-oriented $Pb_{0.4}Sr_{0.6}TiO_3$ thin film sputtered on $LaNiO_3$ electrode, Journal of Crystal Growth 347 (2012) 15–18.
[7] T.D. Cheng, X.G. Tang, Y. Wang, H.L.W. Chan, Strong magnetoelectric coupling in solegel derived multiferroic $(Pb_{0.76}Ca_{0.24})TiO_3$–$CoFe_2O_4$ composite films, Solid State Sciences 14 (2012) 1492–1495.
[8] M. Fu, Q.G. Chi, X. Wang, Y. Chen, Q.Q. Lei, Microstructure and electric properties of $(Pb_{0.8}Ca_{0.2})TiO_3$ thin films prepared by rf magnetron sputtering with a seed layer, Materials Letters 80 (2012) 20–22.
[9] M.L. Calzada, I. Bretos, R. Jimenez, J. Ricote, J. Mendiola, X-ray characterisation of chemical solution deposited $PbTiO_3$ films with high Ca doping, Thin Solid Films 450 (2004) 211–215.
[10] M. Algueró, M.L. Calzada, A.J. Bushby, M.J. Reece, Ferroelectric hysteresis loops of (Pb,Ca)TiO_3 thin films under spherical indentation, Applied Physics Letters 85 (2004) 2023–2025.
[11] M.J. Martın, J. Mendiola, C. Zaldo, Influence of deposition parameters and substrate on the quality of pulsed-laser-deposited $Pb_{1-x}Ca_xTiO_3$ ferroelectric films, Journal of the American Ceramic Society 81 (1998) 2542–2548.
[12] S. Chopra, S. Sharma, T.C. Goel, R.G. Mendiratta, Effect of annealing temperature on microstructure of chemically deposited calcium modified lead titanate thin films, Applied Surface Science 230 (2004) 207–214.
[13] H. Suzuki, Y. Miwa, H. Miyazaki, M. Takahashi, T. Ota, Chemical solution deposition of conductive $SrRuO_3$ thin film on Si substrate, Ceramics International 30 (2004) 1357–1360.
[14] J. Jiang, H.-H. Hwang, W.-J. Lee, S.-Gil Yoon, Microstructural and electrical properties of $0.65Pb(Mg_{1/3}Nb_{2/3})O_3$–$0.35PbTiO_3$(PMN–PT) epitaxial films grown on Si substrates, Sensors and Actuators B 155 (2011) 854–858.
[15] J. Jiang, S.-G. Hur, S.-G. Yoon, Electrical properties of epitaxial 0.65Pb$(Mg_{1/3}Nb_{2/3})O_3$–$0.35PbTiO_3$ thin films grown on buffered Si substrates by pulsed laser deposition, International Journal of Applied Ceramic Technology 8 (2011) 1393–1399.
[16] S. Takahara, A. Morimoto, T. Kawae, M. Kumeda, S. Yamada, S. Ohtsubo, Y. Yonezawa, Fatigue-resistant epitaxial Pb(Zr,Ti)O_3 capacitors on Pt electrode with ultra-thin $SrTiO_3$ template layers, Thin Solid Films 516 (2008) 8393–8398.
[17] L. Qiao, X. Bi, Effect of substrate temperature on the microstructure and transport properties of highly (100)-oriented $LaNiO_{3-\delta}$ films by pure argon sputtering, Journal of Crystal Growth 310 (2008) 3653–3658.
[18] S. Dutta, A. Pandey, I. Yadav, O.P. Thakur, R. Laishram, R. Pal, R. Chatterjee, Improved electrical properties of $PbZrTiO_3$/$BiFeO_3$ multilayers with ZnO buffer layer, Journal of Applied Physics 112 (2012) 0841011–0841016.
[19] R. Ranjith, A.R. Chaudhuri, S.B. Krupanidhi, P. Victor, Role of template layer on microstructure, phase formation and polarization behavior of ferroelectric relaxor thin films, Journal of Applied Physics 101 (2007) 1041111–1041119.
[20] X.G. Tang, H.L.W. Chan, A.L. Ding, Electrical properties of $(Pb_{0.76}Ca_{0.24})TiO_3$ thin Films on $LaNiO_3$ coated Si and fused quartz substrates prepared by a sol–gel process, Applied Surface Science 207 (2003) 63–68.
[21] L.N. Gao, S.N. Song, J.W. Zhai, X. Yao, Z.K. Xu, Effects of buffer layers on the orientation and dielectric properties of $Ba(Zr_{0.20}Ti_{0.80})O_3$ thin films prepared by sol–gel method, Journal of Crystal Growth 310 (2008) 1245–1249.
[22] G.S. Wang, X.J. Meng, J.L. Sun, Z.Q. Lai, J. Yu, S.L. Guo, J.G. Cheng, J. Tang, J.H. Chu, $PbZr_{0.5}Ti_{0.5}O_3$/$La_{0.5}Sr_{0.5}CoO_3$ heterostructures prepared by chemical solution routes on silicon with no fatigue polarization, Applied Physics Letters 79 (2001) 3476–3478.
[23] S. Song, J. Zhai, X. Yao, Effects of buffer layer on the dielectric properties of $BaTiO_3$ thin films prepared by sol–gel processing, Materials Science and Engineering: B 145 (2007) 28–33.
[24] F. Wu, X.M. Li, W.D. Yu, X.D. Gao, X. Zhang, Growth of $La_{0.5}Sr_{0.5}$-CoO_3 thin film on MgO-buffered Si substrate by pulsed laser deposition method: evolution of crystalline orientation, morphology and growth mode with substrate temperature, Journal of Crystal Growth 307 (2007) 367–371.
[25] H.-F. Cheng, Y.-C. Chen, C.-C. Chou, K.-C. Chang, C.-S. Hou, I.-N. Lin, Comparison on the effect of $La_{0.5}Sr_{0.5}MnO_3$ and $La_{0.5}Sr_{0.5}CoO_3$ buffer layers on fatigue properties of $Pb_{0.6}Sr_{0.4}TiO_3$ thin films prepared by pulsed laser deposition, Journal of Applied Physics 87 (2000) 8695–8699.
[26] F.M. Pontes, D.S.L. Pontes, E.R. Leite, E. Longo, E.M.S. Santos, S. Mergulhão, A. Chiquito, P.S. Pizani, F. Lanciotti Jr., T.M. Boschi, J.A. Varela, Influence of Ca concentration on the electric, morphological, and structural properties of (Pb,Ca)TiO_3 thin films, Journal of Applied Physics 91 (2002) 6650–6655.
[27] W.W. Li, Z.G. Hu, Y.W. Li, M. Zhu, Z.Q. Zhu, J.H. Chu, Growth, microstructure, and infrared-ultraviolet optical conductivity of $La_{0.5}Sr_{0.5}$-CoO_3 nanocrystalline films on silicon substrates by pulsed laser deposition, Applied Materials and Interfaces 2 (2010) 896–902.
[28] S. Song, J. Zhai, X. Yao, Enhanced dielectric properties of LSCO-buffered $Ba(Sn_{0.05}Ti_{0.95})O_3$ thin film prepared by sol–gel processing, Journal of Sol–Gel Science and Technology 44 (2007) 75–79.
[29] R.S. Katiyar, Y.I. Yuzyuk, Stress manipulation in ferroelectric thin films and superlattices, Vibrational Spectroscopy 45 (2007) 108–111.
[30] D.A. Tenne, X. Xi, Raman spectroscopy of ferroelectric thin films and superlattices, Journal of the American Ceramic Society 91 (2008) 1820–1834.
[31] P. Khare, D. Sa, Surface effects and diffusive phase transition in ferroelectric thin films: a self-consistent approach, Solid State Communications 152 (2012) 1572–1576.
[32] O.E. Kvyatkovski, Polarization mechanism of ferroelectric lattice instability in crystals, Physics of the Solid State 39 (1997) 602–608.
[33] S. Aggarwal, S.R. Perusse, C.W. Tipton, R. Ramesh, H.D. Drew, T. Venkatesan, D.B. Romero, V.B. Podobedov, A. Weber, Effect of hydrogen on (Pb,Zr)TiO_3-based ferroelectric capacitors, Applied Physics Letters 73 (1998) 1973–1975.
[34] L. Sun, Y.-F. Chen, L. He, C.-Z. Ge, D.-S. Ding, T. Yu, M.-S. Zhang, N.-B. Ming, Phonon-mode hardening in epitaxial $PbTiO_3$ ferroelectric thin films, Physical Review B 55 (1997) 12218–12222.
[35] W.L. Zhua, J.L. Zhu, Y.S. Luo, J.G. Zhu, D.Q. Xiao, R.T. Li, G. Pezzotti, Effect of a $LaSrCoO_3$ buffer layer on $Pb_{1-x}La_xTi_{1-x/4}O_3$ films studied by polarized Raman spectroscopy, Applied Surface Science 256 (2010) 6673–6677.
[36] Yu I. Yuzyuk, Raman scattering spectra of ceramics, films, and superlattices of ferroelectric perovskites: a review, Physics of the Solid State 54 (2012) 1026–1059.
[37] B.G. Chae, Y.S. Yang, S.H. Lee, M.S. Jang, S.J. Lee, S.H. Kim, W. S. Baek, S.C. Kwon, Comparative analysis for the crystalline and ferroelectric properties of Pb(Zr,Ti)O_3 thin films deposited on metallic $LaNiO_3$ and Pt electrodes, Thin Solid Films 410 (2002) 107–113.
[38] A.Z. Simões, M.A. Ramirez, C.R. Foschini, F. Moura, J.A. Varela, E. Longo, Enhanced ferroelectric properties of La-substituted $BiFeO_3$ thin films on $LaSrCoO_3$/Pt/TiO_2/SiO_2/Si(100) substrates prepared by the soft chemical method, Ceramics International 38 (2012) 3841–3849.